Exploring various features of the reaction mechanism involved in the collision of ^{7}Li on Cu

Rishabh Kumar,[1] Moumita Maiti,[1,*] T. N. Nag,[2] and S. Sodaye[2]

[1]*Department of Physics, Indian Institute of Technology Roorkee, Roorkee 247667, Uttarakhand, India*

[2]*Radiochemistry Division and Homi Bhabha National Institute, Bhabha Atomic Research Centre, Mumbai 400085, India*

(Received 8 July 2021; revised 5 October 2021; accepted 26 November 2021; published 9 December 2021)

Nuclear reaction induced by a weakly bound projectile on light-medium mass targets poses open questions on the fusion mechanism. It is seen that fusion suppression in such reactions is negligible, but that stands on the basis of scarcely available experimental data. Thus more experimental data are demanded to bring out a clear understanding. In the course of this, for the first time, a measurement of residual cross sections from ^{7}Li induced reaction on ^{nat}Cu has been presented in this article within the 2.3–6.0 MeV/nucleon energy range. The residues ^{69,67,66}Ge, ^{68,67,66,65}Ga, and ^{69m,65,63}Zn produced in the reaction have been identified by γ-ray spectroscopy. The measured excitation function of the residues has been analyzed using equilibrium and preequilibrium reaction models in the framework of EMPIRE-3.2.2 to understand the reaction mechanisms involved in the low energy region. The underlying reaction mechanism is shown to be a blend of equilibrium and preequilibrium processes. The intensity of the γ peak 93.31 keV arising in the decay of ^{67}Ga has been revised experimentally. The experimental intensity turns out to be about half the value reported in different nuclear databases. Fusion cross sections have been estimated using the experimental data and EMPIRE-3.2.2 code. The estimated fusion cross sections are in line with coupled channel calculations taking inelastic excitations into account. The large production cross section of medically important ^{67}Ga has been measured.

DOI: 10.1103/PhysRevC.104.064606

I. INTRODUCTION

A process as complex as a nuclear reaction offers the undying challenge to experimentalists and theorists to unravel the mysteries lying behind this process. The interaction of two colliding heavy atomic nuclei involves many simultaneously occurring processes involving large degrees of freedom. Over the years, various aspects of nuclear reactions have been discovered with the advent of accelerator and spectroscopy facilities. The study of nuclear reactions has produced more significant consequences in understanding fundamental forces and nucleosynthesis, which has led to the present-day world. It has also provided a new direction in the applied fields, especially in the medical and energy sectors. The availability of heavy-ion (HI) beams ($A > 4$) has made an enormous impact on nuclear reaction study, particularly in understanding the fusion mechanism. The fusion phenomenon, which refers to the total amalgamation of the projectile (P) and target (T), has been a long-standing topic of research due to the presence of a variety of mechanisms, viz., evaporation/equilibrium (EQ), preequilibrium (PEQ), breakup fusion or incomplete fusion (ICF), quasifission, etc., all of which contribute to the reaction cross section of the fusion process at moderate beam energies. With much new experimental research to expand the nuclear chart, it has become imperative to formulate these processes well as they pose hindrance in the synthesis of superheavy elements (SHEs) [1].

The fusion mechanism dominates in low energy nuclear reactions, of which the compound nuclear/equilibrium process constitutes a significant part. An evaporation residue [a residual nucleus formed through the decay of compound nucleus (CN) via particle/γ emission] can be thought of as a culmination of various processes mentioned above. It poses a question about how one can disentangle these processes and develop a thorough understanding. Fortunately, these processes have been accounted for by employing different models and methods. The Bohr hypothesis laid the foundation for understanding the compound nuclear process, which was later developed into a full-fledged statistical theory of compound nuclear decay [2]. Pre-equilibrium emissions, which are primarily characterized as the emission of light and fast particles (LFPs) prior to attainment of statistical or thermodynamic equilibrium of the composite system, were reported in terms of observation of a high energy component in the particle emission spectra and also the presence of a high energy ($>$10 MeV/A) tail in the excitation function [3–5]. Preequilibrium emissions were usually associated with high incident projectile energies, but later observations of these emissions were also reported for energies $<$10 MeV/A [6–8]. However, the experimental data for these are scarce.

ICF was first reported as a massive transfer process with the observation of forward peaked high energy α particles in the intermediate energy heavy-ion induced (primarily ^{12,13}C, ^{16,18}O, etc.) reactions leading to substantial partial fusion as an effect of merging of the remaining part of a projectile with the target [9–11]. The introduction of weakly bound stable

*Corresponding author: moumita.maiti@ph.iitr.ac.in

projectiles (such as ^{6,7}Li, ^{9}Be, also called WBPs) and unstable projectiles (^{11}Li, ^{7,11}Be, ^{8}B), often termed radioactive ion beams (RIBs), opened up a new phase in the nuclear reaction field as their low breakup thresholds and cluster structure makes fusion mechanism multifaceted [12–16]. The experimental challenges arising in dealing with RIBs give way to stable weakly bound beams to properly characterize the reaction mechanism with better statistical data that can be used to compare reaction quantities obtained from the RIBs in the future. ^{6,7}Li beams, owing to their very low breakup thresholds, 1.48 and 2.45 MeV, respectively, have been pervasively used to date in studying fusion mechanisms with WBPs [17–23]. The direct breakup component of ^{6,7}Li after inelastic excitation, $^{6}\text{Li} = \alpha + d$ and $^{7}\text{Li} = \alpha + t$, in reactions with low and medium mass targets was found to be rather weak when compared to reactions with heavy mass targets [24]. Also, it has been put forth that breakup followed by nucleon transfer process ($1n$ stripping for ^{6}Li and $1p$ pickup for ^{7}Li) as well as direct transfer becomes rather significant for the reaction of these beams with medium mass targets [21,24–26].

The enhancement in the complete fusion (CF) cross section at sub-barrier energies, hindrance in the deep sub-barrier, and suppression in the above-barrier region have been reported for the weakly bound stable projectiles [27]. CF suppression in reactions dealing with WBPs has been said to arise mainly due to incomplete fusion. No or scant suppression in the complete fusion cross section has been noticed in the existing literature on the weakly and tightly bound projectile-induced reactions on light and medium-light mass targets. ICF has been shown as a compelling channel in the fusion of ^{6}Li and ^{7}Li projectiles in different target masses [28–32]. However, the amount of complete fusion suppression at higher energies varies with the mass of the target, and CF has been found to be suppressed by $\approx$ 15–30% compared to coupled channels (CC) calculations without considering breakup and transfer couplings [19,22]. However, no suppression in the fusion cross section was reported for ^{7}Li induced reaction on ^{59}Co and ^{64}Zn targets by Beck *et al.* [18] and Di Pietro *et al.* [33], respectively. The absence of noncapture breakup-related suppression in the total fusion cross section (i.e., taking both CF and ICF into account) at energies above the barrier seems to be a prevalent attribute of ^{6,7}Li induced reactions, irrespective of the target mass [18]. There exist only a few measurements of fusion cross section employing ^{7}Li projectile and light-medium mass targets [18,21,33,34], and they suggest that the underlying reaction mechanism of such weakly bound beam is rather complex and a combination of various distinct processes. Thus, the light-medium mass target region demands more experimental data with ^{7}Li beams to shed more light on the reaction mechanism.

Our group also has been involved in exploring the fusion dynamics of light and heavy-ion induced reactions below 10 MeV/nucleon energy [30–32,35–39] with a focus on exploring viable production routes to achieve maximum as well as pure yield for application-based radionuclides [40–46]. In this article, we report the experimental evaporation residue cross sections obtained from the $^{7}\text{Li} + {}^{\text{nat}}\text{Cu}$ reaction at low energies. An effort to explore the production possibility of ^{67}Ga radionuclide, which finds application in radionuclidic imaging, from this reaction has been made. A detailed analysis of the data has been carried out to understand the reaction mechanisms and the behavior of the fusion process involved in the present case. The experimental procedure and brief description of the nuclear model calculations are presented in Secs. II and III, respectively. Section IV discusses the results of the study, and finally Sec. V concludes the report.

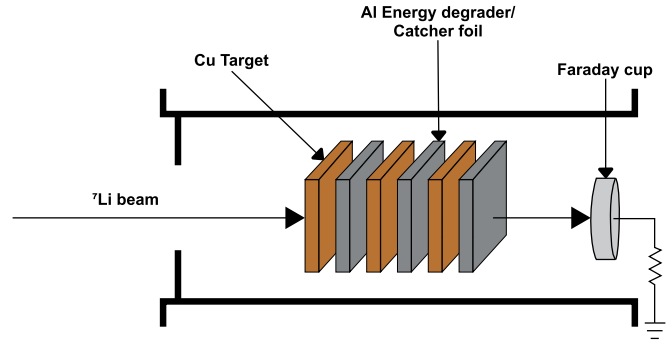

FIG. 1. A schematic diagram of the target stack-foil assembly used for the ^{7}Li + Cu experiment.

II. EXPERIMENTAL DETAILS

The experiment was performed using ^{7}Li-ion beam up to 42 MeV energy delivered by the BARC-TIFR Pelletron Accelerator facility, Mumbai, India. Self-supporting Cu foils of 2.67 mg/cm^2 thickness and Al foils of 1.5–1.6 mg/cm^2 thickness were prepared by properly rolling the spectroscopically pure (99.99%) natural copper ($^{\text{nat}}$Cu) (isotopic abundance: $^{63}\text{Cu} = 69.15\%$ and $^{65}\text{Cu} = 30.85\%$) and aluminum (^{27}Al) metal foils. The $^{7}\text{Li}^{3+}$-ion beam was made to impinge on the copper targets backed by Al foils arranged in a stack. A total of four Cu-Al stacks, each of which contained three Cu foils interspersed with Al, were irradiated by varying the incident energy of $^{7}\text{Li}^{3+}$ ions to have a decent number of energy points between two consecutive irradiations. Al foils fulfilled the purpose of an energy degrader and a catcher for recoils, if any, in the beam direction. A schematic diagram of this stack foil assembly is presented in Fig. 1. The time duration of irradiations was chosen according to the beam intensity and half-lives of the products in mind. Energy degradation in each foil was estimated by Stopping and Range of Ions in Matter (SRIM) code [47] and the typical energy loss in a 2.67 mg/cm^2 thick Cu target was found to be $\approx$ 0.95–1.71 MeV and that in a 1.6 mg/cm^2 Al foil was $\approx$ 0.7–1.25 MeV, depending on the incident energy. The projectile energy at a target is estimated by averaging the incident and outgoing beam energies. The beam current was almost constant during each irradiation, and the total dose of each irradiation (average total dose $\approx$ 304 μC) was measured by an electron-suppressed Faraday cup situated at the rear of the target assembly.

Following the irradiation, each Cu-Al (target-catcher) assembly was assayed using offline γ-ray spectroscopy in a regular interval over a long time using a large volume high-purity germanium (HPGe) detector coupled with a PC

TABLE I. Nuclear spectroscopic data [50] of the residues produced in the ^{7}Li + ^{nat}Cu reaction.

Residue	J^{π}	Half-life	Decay mode (%)	E_{γ} (keV)	I_{γ} (%)
^{69}Ge	$5/2^{-}$	39.05 h	$\epsilon^{a} + \beta^{+}$ (100)	574.11	13.3
				871.98	11.9
				1106.77	36.0
^{67}Ge	$1/2^{-}$	18.9 min	$\epsilon + \beta^{+}$ (100)	167.01	84.0
				1472.8	4.90
^{66}Ge	0^{+}	2.26 h	$\epsilon + \beta^{+}$ (100)	108.85	10.6
				272.97	10.6
				381.85	28.3
^{68}Ga	1^{+}	67.71 min	$\epsilon + \beta^{+}$ (100)	1077.34	3.22
^{67}Ga	$3/2^{-}$	3.2617 d	ϵ (100)	93.31	38.81
				184.576	21.41
				300.217	16.64
^{66}Ga	0^{+}	9.49 h	$\epsilon + \beta^{+}$ (100)	833.5234	5.9
				1039.22	37.0
^{65}Ga	$3/2^{-}$	15.2 min	$\epsilon + \beta^{+}$ (100)	115.09	54.0
				153.0	8.9
				751.8	8.1
^{69m}Zn	$9/2^{+}$	13.756 h	IT^{b} (99.97)	438.63	94.85
			β^{-} (0.03)		
^{65}Zn	$5/2^{-}$	243.93 d	$\epsilon + \beta^{+}$ (100)	1115.539	50.04
^{63}Zn	$3/2^{-}$	38.47 min	$\epsilon + \beta^{+}$ (100)	669.62	8.2
				962.06	6.5

[a]Electron capture.
[b]Isomeric transition.

operating with GENIE-2K software (Canberra). The detector was precalibrated using standard sources, ^{152}Eu (13.506 y), ^{137}Cs (30.08 y), and ^{60}Co (5.27 y) of known activity. The energy resolution of the detector was 2.0 keV at the 1332 keV energy γ ray of ^{60}Co. The populated residues were identified by their characteristic γ rays and decay profiles obtained from the recorded spectra. The yield of residue is measured from the background-subtracted peak area count of a particular γ-ray energy [48]. The cross section of a particular evaporation residue at incident energy E has been evaluated using the activation formula [30,49]. The nuclear spectroscopic data used to calculate the evaporation residue's production cross sections are listed in Table I [50].

The associated uncertainties in the cross section measurement may arise from the following: (i) uncertainty of 2% in the geometry-dependent efficiency of the detector, (ii) nonuniformity of target thickness leading to an error of 2%, (iii) uncertainty in the beam flux due to fluctuation in beam current, estimated to be 7%, (iv) statistical error in the background-subtracted peak area count being different for different residues and propagated to the cross section measurement, although dead time was kept $\leqslant 8\%$, (v) error in the estimation of beam energy due to the degradation of energy while traversing through the successive target foils; however, energy straggling effects are expected to be small [51]. The average estimated error was $\approx 13\%$ taking all the factors into account, although it rose to $\approx 20\%$ for a few cases, where counting statistics were low. The incident projectile energy assigned to each foil has an associated uncertainty that includes an error in the SRIM calculation and the determination of target thickness.

III. MODEL CALCULATION

EMPIRE-3.2.2 [52] is a versatile modular nuclear reaction code that incorporates all three major reaction processes—equilibrium (EQ), preequilibrium (PEQ), and direct (DIR)—into its formalism and was particularly designed for calculations over a broad range of energies and incident particles. EMPIRE has been used to understand the reaction mechanism of the present reaction ^{7}Li + Cu. The Hauser-Feshbach model, including width fluctuations, deals with EQ processes, whereas PEQ processes are taken care of using a phenomenological PEQ model, the exciton model. It employs the coupled channels (CC) method and distorted-wave Born approximation (DWBA) to estimate contributions from direct reactions. The heavy-ion fusion cross section has been estimated using the coupled channels code CCFUS [53] that takes into account the inelastic excitations and transfer reaction channels independently that couple to the initial ground state. In the present study, we used the exciton model with mean free path parameter 1.5 (mean free path is the distance a nucleon travels inside the nuclear matter between successive collisions) and the Hauser-Feshbach formalism to estimate a residue's PEQ and EQ cross sections, respectively. The PCROSS module is used to incorporate the exciton model into the main EMPIRE code for pre-equilibrium nucleon emission with a further provision of including the preequilibrium mechanism for cluster emission based on the Iwamoto-Harada model. In the code, the transmission coefficients of particle emissions have been obtained using an optical model. The optical model parameters used for the neutron and proton were taken from Koning and Delaroche [54], for the deuteron from

Haixia *et al.* [55], for the triton and ^{3}He from Becchetti and Greenless [56], and those for α particles from Avrigeanu *et al.* [57].

The role of level-density models in cross section estimation of residues is quite essential in nuclear reactions. We have used the Gilbert-Cameron (GC) model, the generalized superfluid model (GSM), and enhanced generalized superfluid model (EGSM) level densities to bring out the effect and relevance of level density on the underlying reaction mechanism. These models are based on Fermi gas model (FGM), each treating the level density in different energy schemes. The GC model uses the constant temperature formula of level density at low excitation energies (below the matching energy U_x) and the Fermi gas model above U_x. The functional form of FGM level density is as follows:

$$\rho^{\mathrm{FG}}(E_x, J, \pi) = \frac{2J+1}{48\sqrt{2}\sigma^{3/2}a^{1/4}U^{5/4}} \times \exp\left[2\sqrt{aU} - \frac{(J+1/2)^2}{2\sigma^2}\right], \quad (1)$$

where U is the effective excitation energy ($U = E_x - \Delta$), a is the level density parameter, σ^2 is the spin cutoff parameter, and lastly J and π are spin and parity of intrinsic levels. Δ is equal to or closely related to the pairing energy to account for even-odd effects. The a parameter has an energy dependence that arises from its relation with shell corrections and the fade-out of these shell effects with increasing excitation energy. In the GC model, this a parameter can be deduced from the systematics proposed by Ignatyuk *et al.* [58], Young *et al.* [59], and Iljinov *et al.* [60]. For the present case, systematics provided by Iljinov *et al.* has been used in the calculations. The GSM is characterized by a phase transition from a low-energy to a high-energy region split apart by the critical excitation energy, U_c. At low energy, the superfluid behavior is dominant, where pairing correlations strongly influence the level densities, while, at high energy, the FGM is used to describe the level densities. Below U_c, the level densities are calculated in the framework of the BCS model, and the superconducting pairing correlations are considered in terms of the correlation function δ_0. The EGSM (EMPIRE specific level density), similarly to GSM, is based on the Fermi gas model level density in an adiabatic mode along with a collective enhancement factor which damps out with increasing excitation energy (E_x) and reduces to unity above a critical temperature T_c. In EGSM, the critical level density parameter (a_c) is used below T_c and the Ignatyuk empirical level density parameter, defined as

$$a(E_x) = \tilde{a}\left[1 + \frac{\delta W}{U^*}(1 - e^{-\gamma U^*})\right], \quad (2)$$

is used above T_c, where $\tilde{a} = 0.0748A$ and $\gamma = 0.5609A^{1/3}$ are the asymptotic values of the a parameter and the shell effect damping parameter, respectively. δW is the shell correction factor which fades out with increasing excitation energy (E_x) and $U^* = U - 0.1521a_c\delta_0^2$ is the effective excitation energy above T_c. The correlation function δ_0 is calculated as $\delta_0 = 12/\sqrt{A}$. Enhancement compared to GSM relates mainly to incorporating spin distribution in the Fermi gas model and better treatment of the collective (vibrational/rotational) enhancements arising from nuclear rotation. Level densities acquire dynamic features through the dependence of the rotational enhancement on the shape of the nucleus, and the deformation enters the level densities formula through the moment of inertia. The EGSM adopts a much accurate treatment of angular momentum, which is more suitable for heavy-ion induced reactions than the other two.

IV. RESULTS AND INTERPRETATION

The analysis of time-resolved γ-ray spectra collected after the end of bombardment (EOB) revealed that the ^{7}Li-induced reaction on $^{\mathrm{nat}}$Cu ensured production of ^{69,67,66}Ge, ^{68,67,66,65}Ga, and $^{69\mathrm{m},65,63}$Zn in the target matrix within the 16–42 MeV incident energy range. A typical γ-ray spectrum of the evaporation residues produced in the ^{7}Li irradiated Cu target at 38.1 MeV incident energy, collected 23.0 minutes after the EOB, is shown in Fig. 2 with each residue marked with its characteristic γ rays in keV. Figure 3 shows the decay profiles of ^{69}Ge and ^{68}Ga along with their half-lives obtained from the fits to decay profiles. The cross section of the evaporation residues at various energies is presented in Table II. The experimental excitation functions of the residues are compared with those obtained theoretically from the model code EMPIRE-3.2.2 [52], as shown in Figs. 4, 5, and 7. Experimental data are shown by symbols with an error bar, whereas lines show theoretical calculations. The results from different reaction channels have been discussed below in detail.

A. *xn* channel

The ER cross sections obtained from the reaction ^{63,65}Cu(^{7}Li, xn)^{k}Ge ($k = 69, 67, 66$) in the 16–42 MeV energy range are presented in Fig. 4. The measured excitation function for ^{69}Ge is compared with those obtained from EMPIRE employing different level densities in Fig. 4(a). It can be affirmed that the trend of the experimental cross sections is adequately reproduced by EMPIRE calculations with all three level densities. It is quite evident from Fig. 4(a) that EMPIRE with EGSM level density more accurately predicts the experimental data throughout the measured energy range. The calculations with GC and GSM level density slightly overpredict the data at energies lower than 30 MeV, but their estimations are in close proximity to the experimental data at higher energies. Also shown are the excitation functions corresponding to EMPIRE (with EGSM) calculated ^{69}Ge production from ^{63}Cu(^{7}Li, n) (orange dash-dotted line) and ^{65}Cu(^{7}Li, $3n$) (black dotted line), which reveal that the major contribution to ^{69}Ge production comes from the ^{7}Li + ^{65}Cu reaction. To understand the relative contribution from the ^{63}Cu and ^{65}Cu targets, the individual theoretical excitation functions for EGSM level density will be shown for the residual radionuclides. Figure 4(b) shows a comparison of measured and theoretical excitation functions of ^{67}Ge. It can be noticed that the estimates of EMPIRE in the lower energy bracket with EGSM (solid blue line), GC (red dashed line), and GSM (green dotted line) level density agree reasonably well with the experimental data. Although EGSM and GC calculations match the experimental data at higher energies, GSM level

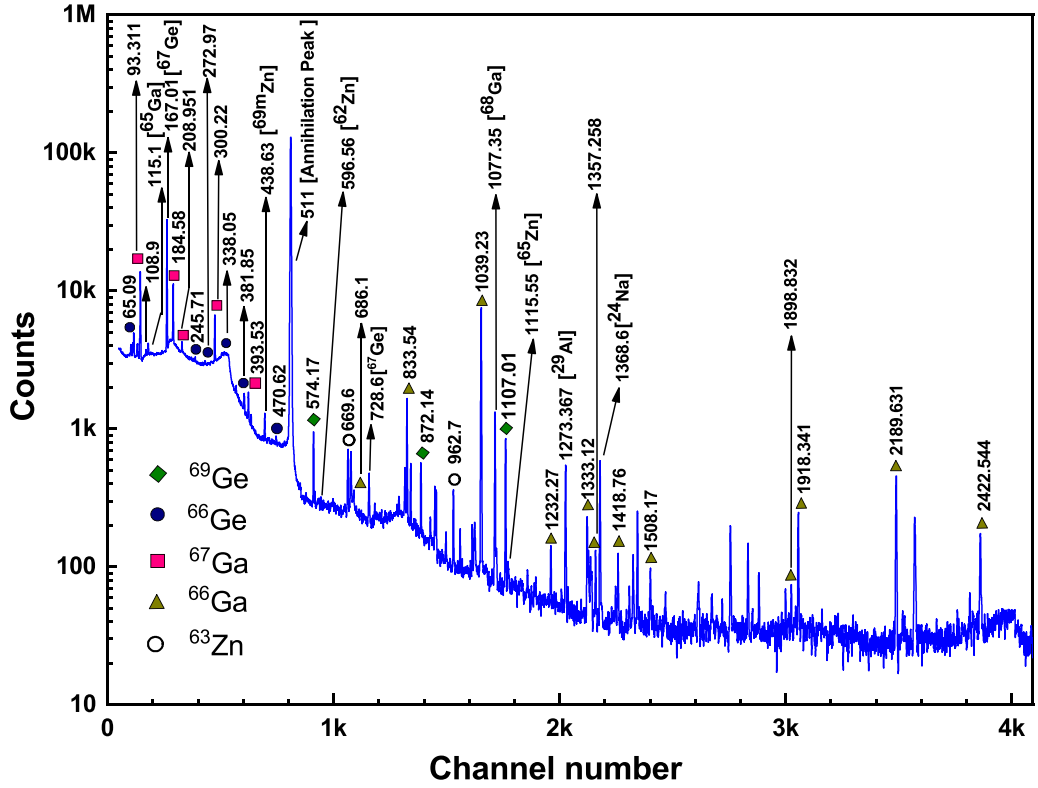

FIG. 2. A typical γ-ray spectrum of 38.1 MeV ^{7}Li irradiated ^{nat}Cu target collected 23.0 min after the EOB. The γ-ray energies, shown in the spectrum, are in keV.

density presents lower cross sections than the experimental ones. The individual contributions of ^{63}Cu and ^{65}Cu targets to ^{67}Ge production show the dominance of the ^{63}Cu(^{7}Li, $3n$) channel, which can be noted from the fact that the cross

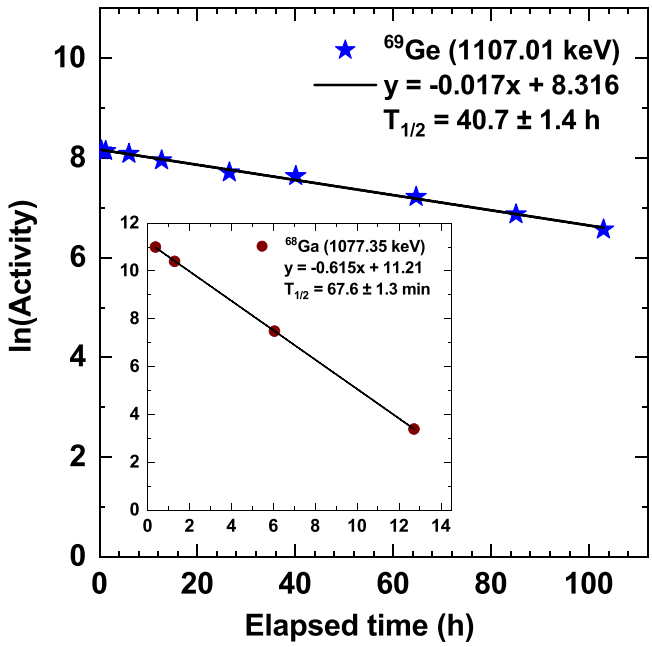

FIG. 3. Half-life estimates from decay curve analysis of ^{69}Ge and ^{68}Ga (see inset).

section trend matches with the experimental data. Anew, experimentally obtained excitation function of ^{66}Ge, depicted in Fig 4(c), is well reproduced by EMPIRE with EGSM level density. In contrast, GSM level density underpredicts the data, and the cross sections obtained from GC level density are slightly higher than the experimental data. Here again, the production of ^{66}Ge is solely from the ^{63}Cu(^{7}Li, $4n$) reaction channel.

On qualitative grounds from the results of *xn* channel, it can thus be emphasized that EMPIRE with EGSM level density explicitly explains the *xn* channel cross sections, which are predominantly produced via the complete fusion mechanism. The deviation of GSM level density calculations in Figs. 4 (b) and (c) might be due to the fact that it does not take into account the spin distribution in the Fermi gas model and so, above the critical excitation energy, fails to predict the level densities better. Also, the EGSM and GSM define the effective excitation energy used in level density calculations differently, possibly leading to their differences in calculating level densities. It is also worth noting that the underlying reaction mechanism present for the *xn* channel is the compound nuclear and preequilibrium decay following the satisfactory reproduction of the experimental data by theoretical calculations comprising both statistical compound and PEQ models.

B. *pxn* channel

The complete fusion of ^{7}Li in Cu and the subsequent decay of compound nuclei through proton emission ($p/d/t$-xn)

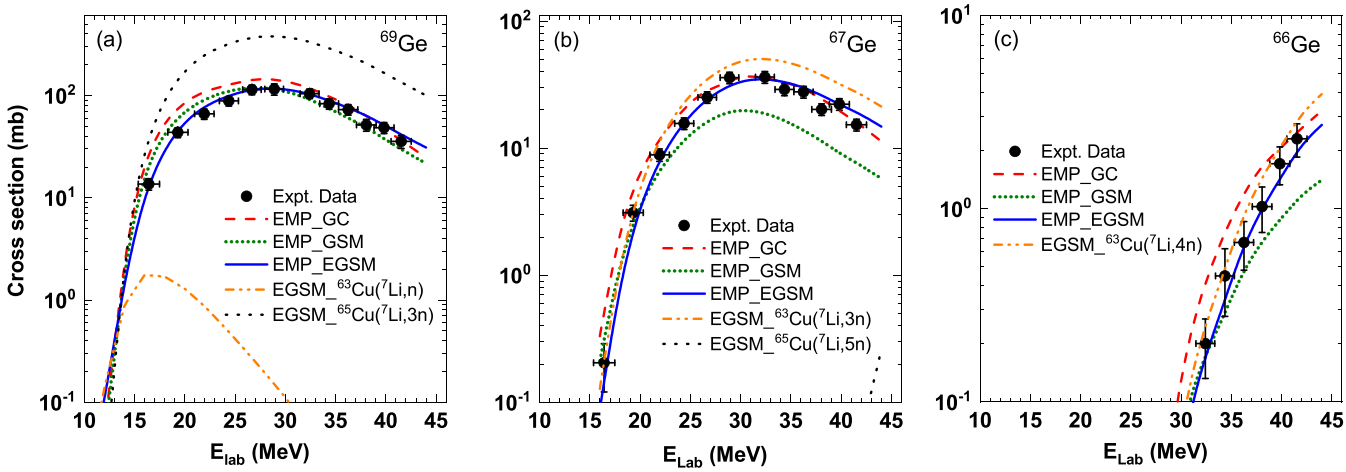

FIG. 4. Comparison of experimental excitation functions (black solid circles) of *xn* channel residues: (a) ^{69}Ge, (b) ^{67}Ge, and (c) ^{66}Ge from the ^{7}Li + ^{nat}Cu reaction, and those obtained from theory using EMPIRE (curves).

channels leads to the formation of ^{68}Ga, ^{67}Ga, ^{66}Ga, and ^{65}Ga residues, whose EFs are presented in Fig. 5. It can be observed from Fig. 5(a) that the trend of the ^{68}Ga excitation function offered by EMPIRE with the three level densities is similar to the measured one, but estimates of the cross section from calculations with EGSM level density are more in line with experimental cross sections. While at lower energies, below 30 MeV, EMPIRE with GC and GSM level densities agree with the data, they start overpredicting the data at energies above 30 MeV. This overprediction might again be

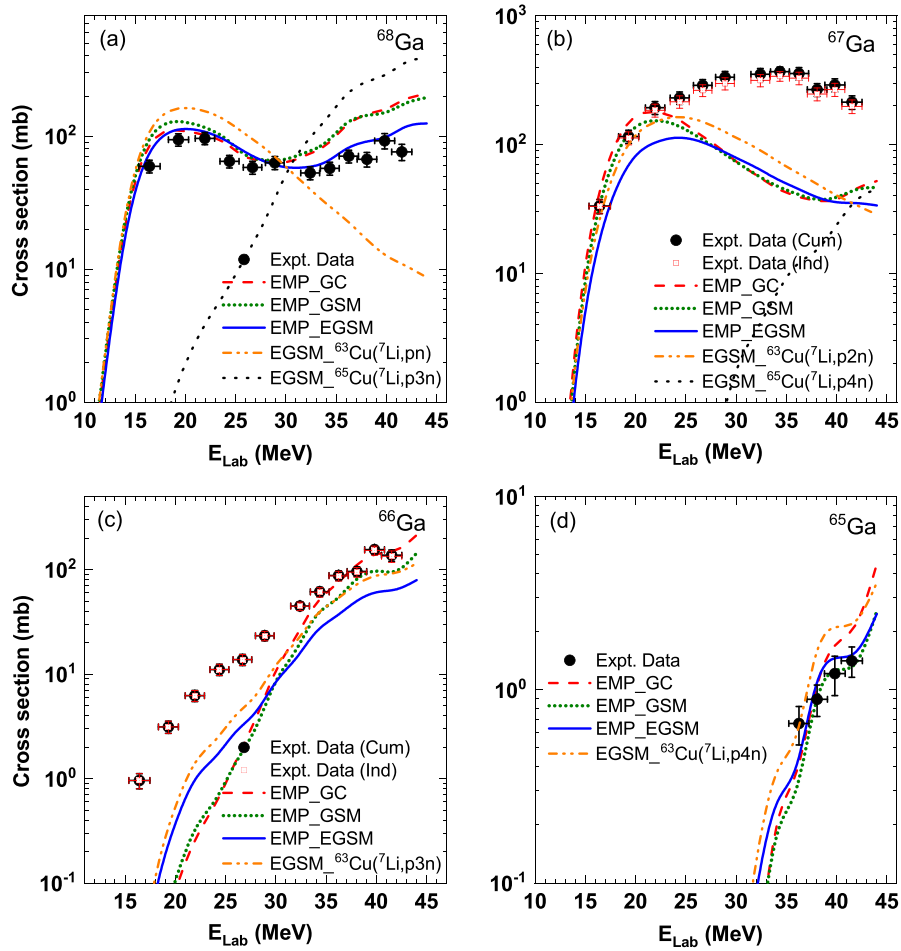

FIG. 5. Same as Fig. 4 but for (a) ^{68}Ga, (b) ^{67}Ga, (c) ^{66}Ga, and (d) ^{65}Ga residues populated through the *pxn* channel.

TABLE II. Cross sections (mb) of residues produced in ^{7}Li + ^{nat}Cu reaction at different incident energies.

	Cross section (mb)									
Energy (MeV)	^{69}Ge	^{67}Ge	^{66}Ge	^{68}Ga	^{67}Ga$_{Cum}$	^{66}Ga$_{Cum}$	^{65}Ga	^{69m}Zn	^{65}Zn$_{Cum}$	^{63}Zn
16.4 ± 1.1	13.6 ± 2.7	0.2 ± 0.1		59.3 ± 6.5	33.3 ± 4.1	1.0 ± 0.2			48.1 ± 13.1	
19.3 ± 1.0	43.6 ± 4.8	3.1 ± 0.4		94.1 ± 10.1	115.8 ± 13.5	3.1 ± 0.4			87.9 ± 18.2	
21.9 ± 1.0	66.1 ± 7.6	8.9 ± 1.0		96.2 ± 10.1	193.7 ± 22.2	6.2 ± 0.8		0.2 ± 0.1	111.2 ± 21.6	
24.4 ± 0.9	88.4 ± 9.5	15.7 ± 1.6		64.5 ± 7.0	230.7 ± 25.2	11.1 ± 1.4		0.3 ± 0.1	105.3 ± 27.1	
26.7 ± 0.9	113.9 ± 12.2	25.2 ± 2.6		58.2 ± 6.5	289.1 ± 30.4	13.7 ± 1.7		0.6 ± 0.1	72.0 ± 19.0	
28.9 ± 0.9	115.3 ± 14.8	35.9 ± 3.7		63.1 ± 7.2	334.2 ± 36.0	23.2 ± 2.4		0.9 ± 0.1	71.2 ± 18.9	
32.4 ± 0.9	104.2 ± 11.2	36.3 ± 3.9	0.2 ± 0.1	52.9 ± 5.9	352.1 ± 38.2	44.9 ± 4.1		1.3 ± 0.2	47.8 ± 14.8	1.1 ± 0.4
34.4 ± 0.9	83.1 ± 9.6	29.1 ± 3.2	0.45 ± 0.2	57.3 ± 6.4	368.9 ± 32.2	61.4 ± 6.2		1.6 ± 0.2	47.1 ± 16.0	3.4 ± 0.7
36.2 ± 1.0	72.8 ± 8.5	27.7 ± 3.0	0.7 ± 0.2	70.6 ± 7.7	356.2 ± 39.7	87.9 ± 9.2	0.7 ± 0.2	1.8 ± 0.2	72.3 ± 18.5	5.6 ± 1.0
38.1 ± 1.0	51.6 ± 6.9	20.2 ± 2.1	1.0 ± 0.3	67.0 ± 8.4	267.3 ± 30.6	96.0 ± 9.9	0.9 ± 0.2	1.5 ± 0.2	64.4 ± 21.4	7.7 ± 1.2
39.8 ± 1.0	48.4 ± 6.0	22.2 ± 2.4	1.7 ± 0.4	92.3 ± 12.2	290.3 ± 33.9	155.1 ± 15.1	1.2 ± 0.3	1.8 ± 0.2	79.0 ± 20.1	15.6 ± 2.0
41.5 ± 1.0	35.6 ± 5.2	15.3 ± 1.6	2.3 ± 0.4	76.1 ± 10.6	213.6 ± 25.7	137.3 ± 17.0	1.4 ± 0.2	1.4 ± 0.2	73.4 ± 28.7	16.5 ± 2.1

due to the underlying differences in the formalism of the three level densities, with EGSM being much superior for high energy heavy-ion induced reactions and being, in fact, the recommended default level density in the manual of the code. It is also interesting to see that at lower energies (below 30 MeV), the ^{63}Cu target is the leading contributor in the production of ^{68}Ga while it is the ^{65}Cu target at the higher energies. The next radionuclide is ^{67}Ga and, before proceeding with the discussion, a brief detail about ^{67}Ga would help one to understand some peculiarities. ^{67}Ga ($T_{1/2}$ = 3.2617 d, $J^{\pi} = 3/2^{-}$) decays via 100% electron capture (EC) to ^{67}Zn. ^{67}Ga is formed via the reactions ^{63}Cu(^{7}Li, $p2n/dn/t$) and ^{65}Cu(^{7}Li, $p4n/d3n/t2n$). The decay of ^{67}Ga corresponds to six strong γ rays found in different nuclear databases [50,61–64]: 91.265 keV ($I_{\gamma} = 3.11\%$), 93.31 keV ($I_{\gamma} = 38.81\%$), 184.576 keV ($I_{\gamma} = 21.41\%$), 208.95 keV ($I_{\gamma} = 2.46\%$), 300.217 keV ($I_{\gamma} = 16.64\%$), and 393.527 keV ($I_{\gamma} = 4.56\%$). There is a slight difference in γ-ray energy/intensity values across the databases. In the present analysis, the measured activities at the EOB (or cross sections) of ^{67}Ga using all other γ rays were consistent, except for 93.31 keV, for each target. The measured radioactivities using 93.31 keV were found to be about half of what is estimated by other γ rays. A possible reason for such an observation can be attributed to the use of incorrect γ-ray peak intensity reported in the databases for cross section calculation. Thus, an experimental estimate of the intensity of 93.31 keV peak has been computed in Sec. IV D.

The EF for ^{67}Ga residue is projected in Fig. 5(b). It can be figured that the experimental cross sections are quite large compared to the EMPIRE calculations beyond 23 MeV. The large cross section could be attributed to the cumulative production of ^{67}Ga, via *pxn* channel and from the decay (EC + β^{+}) of its precursor ^{67}Ge. Independent cross sections of ^{67}Ga have been obtained from the cumulative ones using the prescription proposed by Cavinato *et al.* [5] owing to the fact that the precursor ^{67}Ge ($T_{1/2}$ = 18.9 min; refer to Table I), is quite short-lived as compared to the daughter (^{67}Ga, $T_{1/2}$ = 3.2617 d) nuclide. It is interesting to note from Fig. 5(b) that, even after obtaining independent cross section (red open squares), a stark contrast in the experimental cross section and theoretically calculated excitation function for ^{67}Ga is observed as EMPIRE predicts a decreasing trend of the cross section beyond 23 MeV. However, the calculations offer equivalent cross sections compared to experimental data at energies below 23 MeV.

Similarly to ^{67}Ga, ^{66}Ga is formed via the *pxn* channel and also via the decay (EC + β^{+}) of its precursor ^{66}Ge (refer to Table I for decay information details), and consequently the independent cross sections have been calculated. Figure 5(c) shows the experimental cross section of ^{66}Ga residue along with the EMPIRE estimation, and it is evident from it that, although EGSM level density estimations match the trend of cross sections, it surely underpredicts the data in the whole energy range. The two other level density models do not predict the trend well. However, GC calculations offer an agreement with the experimental data at energies above 35 MeV. It is also worth mentioning here that the cross sections appearing for ^{66}Ga are from ^{7}Li induced reaction on ^{63}Cu

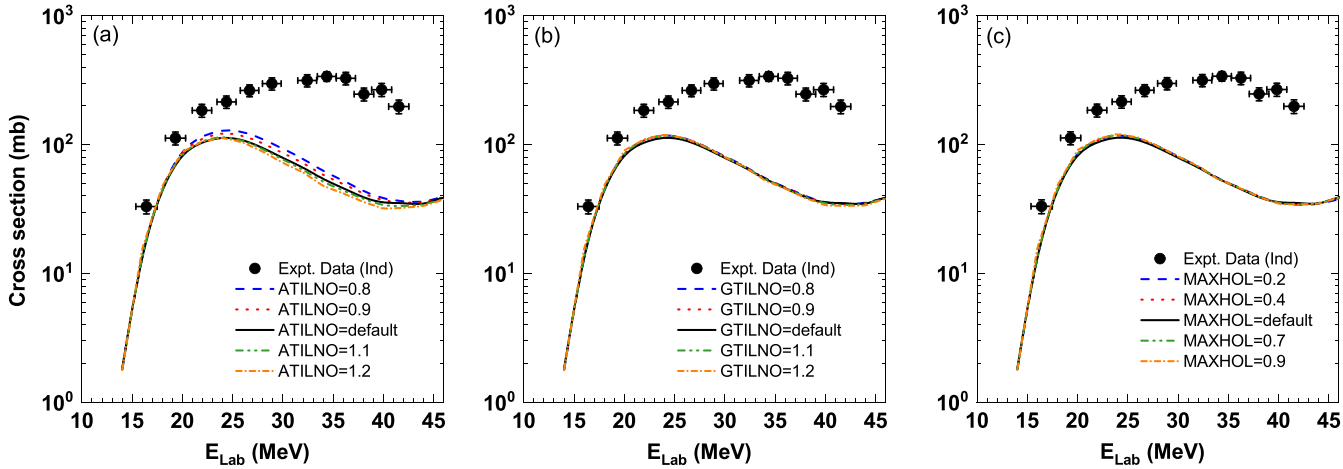

FIG. 6. Effect of variation of different model parameters in EMPIRE on the cross sections of ^{67}Ga. The model parameters have been varied for EGSM level density; the default input parameter calculation has been shown for comparison. Variation of (a) ATILNO parameter in the range 0.8–1.2, (b) GTILNO parameter in the range 0.8–1.2, and (c) MAXHOL parameter in the range 0.2–0.9. The experimental data (black filled circles) are shown for comparison with model computed values (curves). The description of the model parameters in detail can be found in the text.

[see the orange dotted curve in Fig. 5(c)]. The last identified residue produced from the p-emitting channel is ^{65}Ga, whose excitation functions are plotted in Fig. 5(d). We note here that experimental cross sections are precisely reproduced by EMPIRE calculations considering the three level densities and that the ^{63}Cu(^{7}Li, $p4n/d3n/t2n$) reaction is the sole contributor to the production cross sections.

The large deviations found between the experimental data of ^{67}Ga and model calculations indeed demand an investigation in terms of various model input parameters that can be used to check for any abnormality. Motivated by this, we have tried to check the effect of different input parameters on cross sections of ^{67}Ga. First, the manual of the code suggests checking calculations with different level densities, which has already been performed and showcased in Fig. 5(b). Furthermore, the underpredicted cross section might be due to the incorrect fitting of the discrete levels of ^{67}Ga. This fitting can be performed using the FITLEV option, which brought out that the fitting was good. Last, one can vary the ATILNO parameter to change the asymptotic value of level density parameter a, which modifies the densities of the levels of a particular residual nucleus under consideration; for instance, presently on varying ATILNO from 0.8 to 1.2 the asymptotic value of the level density parameter (a) ranges from 4.0 to 6.0 (default value = 5.0). Figure 6(a) shows this variation of the ATILNO parameter (considering EGSM level density) in comparison to the experimental data and exposes that there is no significant change in the theoretical cross sections for different values of the ATILNO parameter while still predicting lower cross sections than the experimental ones. Another possible reason could be the underprediction of PEQ cross sections for ^{67}Ga residue. The PEQ contribution provided by PCROSS code is controlled by two input parameters, viz., GTILNO and MAXHOL, which are the single-particle level density parameters of PEQ emissions for a particular residual nucleus and maximum hole number parameter, respectively. Figure 6(b) shows the calculated excitation functions with varying values of the GTILNO parameter, and it is pretty clear that the cross sections seem insensitive to this parameter's variation. Moreover, Fig. 6(c) puts forward the effect on theoretical cross sections of varying the MAXHOL parameter, which controls the number of holes (and, in turn, the number of excitons). The MAXHOL parameter can be varied between values 0.1 and 1.0, with the default value from systematics being 0.54, and yet again it can be noticed in Fig. 6(c) that there is no enhancement in theoretical cross sections. These arguments suggest that the cross sections of ^{67}Ga internally calculated by EMPIRE are insensitive to the external optional input parameters.

Now, the excess cross sections found in ^{67}Ga and ^{66}Ga compared to theoretical model calculations could be due to other processes not accounted for in the EMPIRE code such as breakup fusion or incomplete fusion and direct cluster transfer (DCT), also known as the massive transfer process. The ^{7}Li incident projectile can breakup ($S_\alpha = 2.47$ MeV) into $\alpha + t$ and the capture of α by Cu can lead to the production of ^{66,67}Ga:

$$\begin{aligned} {}^{7}\mathrm{Li} &\rightarrow \alpha + t, \\ \alpha + {}^{63}\mathrm{Cu} \rightarrow [{}^{67}\mathrm{Ga}^{*}] &\rightarrow {}^{67}\mathrm{Ga} + \gamma, \quad E_{\mathrm{th}} = 0.0\ \mathrm{MeV}, \\ &\rightarrow {}^{66}\mathrm{Ga} + n, \quad E_{\mathrm{th}} = 7.98\ \mathrm{MeV}, \\ \alpha + {}^{65}\mathrm{Cu} \rightarrow [{}^{69}\mathrm{Ga}^{*}] &\rightarrow {}^{67}\mathrm{Ga} + 2n, \quad E_{\mathrm{th}} = 14.97\ \mathrm{MeV}, \\ &\rightarrow {}^{66}\mathrm{Ga} + 3n, \quad E_{\mathrm{th}} = 26.89\ \mathrm{MeV}. \end{aligned} \tag{3}$$

The above thresholds for the reactions correspond to the energy needed by the cluster or the breakup fragment to induce that particular reaction. After breakup, the breakup fragment energy can be thought as $E_{\mathrm{clu}} = (E_p - S_\alpha) \times m_{\mathrm{clu}}/m_p$, where E_p is the incident projectile energy, S_α is the α cluster breakup threshold (= 2.47 MeV for ^{7}Li), and m_{clu} and m_p are the masses of the cluster and projectile, respectively. In the present energy range of 16–42 MeV of ^{7}Li, the E_{clu} for α

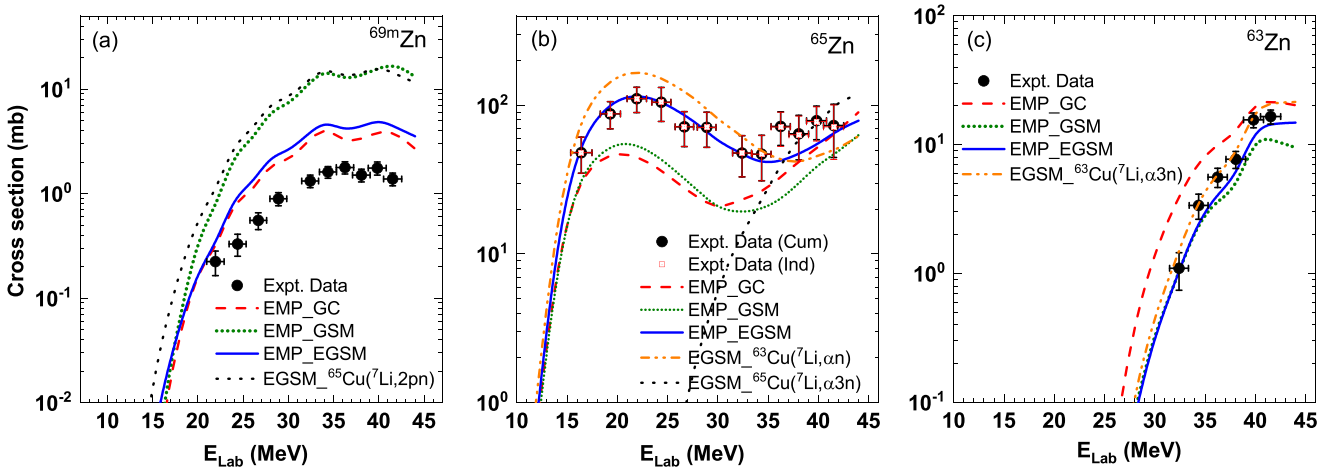

FIG. 7. Same as Fig. 4 but for (a) ^{69m}Zn, (b) ^{65}Zn, and (c) ^{63}Zn populated through the αxn channel.

particles comes out around 8–22 MeV. It suggests that in this energy range of interaction the possible routes to the production of ^{67}Ga and ^{66}Ga are through ^{65}Cu$(\alpha, 2n)$ and ^{63}Cu(α, n), respectively, since for the fourth reaction [refer to Eq. (3)] the threshold is quite high and for the first reaction the excitation energy of ^{67}Ga* would be enough for preferential particle emission to shed that excitation energy apart. This fact has also been confirmed from model calculations (EMPIRE with EGSM) for $\alpha + {}^{63}$Cu and $\alpha + {}^{65}$Cu reactions. It shows that the production cross section for ^{67}Ga via ^{63}Cu(α, γ) is 0 mb and that via ^{65}Cu$(\alpha, 2n)$ varies between 0 and 720 mb (50% of total fusion cross section at peak) in the above mentioned energy range. Accordingly, the production cross section for ^{66}Ga via ^{63}Cu(α, n) varies from 0 to 530 mb (49% of total fusion cross section at peak) and that for ^{65}Cu$(\alpha, 3n)$ is 0 mb.

C. $2p/\alpha xn$ channel

The decay of compound nuclei formed in the ^{7}Li + $^{\text{nat}}$Cu reaction through the $2p/\alpha xn$ channel leads to the production of ^{69m,65,63}Zn residues whose excitation functions are duly represented in Fig. 7. We report the measured cross sections of ^{69m}Zn formed via the ^{65}Cu$(^{7}\text{Li}, 2pn)^{69m}$Zn reaction in Fig. 7(a). Since EMPIRE is capable of estimating the cross sections for isomeric states, those cross sections calculated with different level densities have been compared with the experimental data. It can be observed that EMPIRE estimated cross sections are quite large compared to the measured cross sections, although it correctly predicts the trend of the data. Figure 7(b) shows that the experimental cross sections of ^{65}Zn are well reproduced by EMPIRE with EGSM level density, whereas calculated cross sections with GC and GSM level density lie well below the experimental data, although they predict a similar trend. It can also be keenly observed that the cross sections at lower energy come from the ^{63}Cu target while it is a mixture of both the targets that reproduces the data well at higher energies. Similarly, for ^{63}Zn residue formed via the α emitting channel, the excitation functions obtained experimentally as well as theoretically are plotted in Fig. 7(c). It can be easily seen that EMPIRE with EGSM level density accurately reproduces the experimental cross sections throughout the energy range. Calculations with GC level density slightly overpredict the data, whereas GSM level density shows good agreement with the data except for a small deviation at higher energies. Here too, the major contribution to the production cross section is from reaction with the ^{63}Cu target. The overall comparative analysis of the individual residues reveals the fact that EMPIRE performs consistently and reasonably well in reproducing experimental data of almost all the residues except for a few. Previous works have also emphasized the effectiveness and accuracy of EMPIRE code in engendering valuable understanding of heavy-ion induced reactions in the low and intermediate energy range [7,35,37].

The comparison of the experimental data with theoretical model calculations for the reported residues certainly marks complete fusion as the dominant reaction process in the ^{7}Li + $^{\text{nat}}$Cu reaction. Further, this complete fusion comprises two distinct processes: compound nuclear decay and preequilibrium emissions. The EMPIRE code provides the total contribution (sum of all the reaction products formed) of different reaction processes in its output file, but such a provision is not present separately for each residue formed in the reaction. Figure 8(a) shows the cross sections fed by the compound nuclear process (estimated by statistical Hauser-Feshbach model) and preequilibrium process (by exciton model) into the total nonelastic cross section calculated with EMPIRE using EGSM level density. The CN process is dominant at lower energies, while the preequilibrium cross sections seem to increase with the energy and become comparable to CN at the highest energy. Figure 8(b) shows the relative contribution of CN and PEQ processes, and it can be seen that for most of the energy range the CN is the major contributing partner as it varies from almost 100% to $\approx$ 60%, while the PEQ process only becomes significant at energies above 30 MeV as it varies from 0% to $\approx$ 40%.

In previous studies, reactions involving ^{7}Li projectiles incident on targets of different masses were found to have significant ICF contribution in the total fusion, leading to more CF suppression. The fact that ICF fraction seems to decrease with a decrease in target charge has been put forth in the past decade [14,22]. Apart from having a higher breakup threshold, 2.47 MeV, for ^{7}Li than ^{6}Li (1.47 MeV) to dissociate

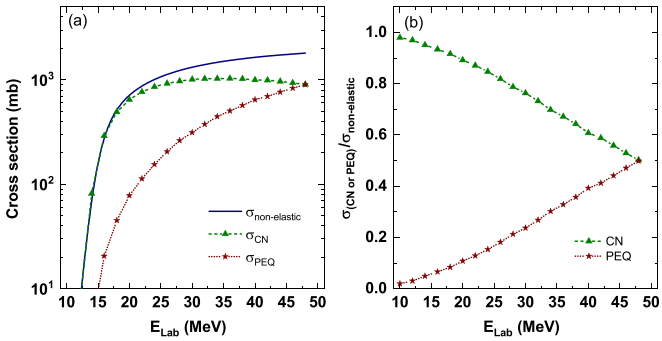

FIG. 8. Contribution of compound nuclear and preequilibrium processes in the fusion cross section within the studied energy range computed from EMPIRE with EGSM level density. (a) Cross sections of different processes: CN (green curve with triangles) and PEQ (brown curve with stars), occurring in the reaction ^{7}Li + ^{nat}Cu. The blue curve represents the total nonelastic cross section. (b) The relative contribution of CN and PEQ processes.

into its cluster constituents, the negligible near-target breakup probability for ^{7}Li in the field of light-heavy targets leads to much less suppression of CF cross sections compared to ^{6}Li, which suggests almost no presence of ICF in the case of ^{7}Li with lighter mass targets [24,34]. Furthermore, it was suggested by Di Pietro *et al.* [33] for ^{6,7}Li + ^{64}Zn reactions that α–ICF/DCT and d/t–ICF/DCT processes largely dominate the fusion mechanism at below barrier energies. At the same time, they were found to be weak at energies far above the barrier, which could also be a possible reason for ICF not entering in the ^{7}Li + ^{nat}Cu reaction, which has been studied at above barrier energies. One can compute the ICF cross section using the data reduction method from the measured ER cross sections as reported in the past [20,30,49]. Following the principles of this method, in the present reaction, comparisons of ER cross sections with EMPIRE reveal no notable enhancement in the p- and α-emitting channels with respect to EMPIRE calculation. The enhanced cross sections of ^{66}Ga above EMPIRE indicates a hint of ICF. However, it would be unwise and difficult to disentangle CF and ICF unambiguously for a single p-emitting channel. We also note a large enhancement in ^{67}Ga cross sections compared to EMPIRE, but this must not be considered as being solely due to ICF since EMPIRE was found to act differently for this particular residue in the ^{6}Li + ^{nat}Cu reaction, as reported by Kumar *et al.* [65] recently. Also, the analysis performed using different input model parameters suggests that the issue needs further investigation into the internal performance of the code for ^{67}Ga produced in Li-induced reactions on light-medium mass targets. All of this implies the existence of a tiny possibility of ICF in a single p-emission channel, and it can be considered that ICF does not hinder the fusion of ^{7}Li into Cu.

D. Determination of intensity of 93.31 keV γ ray of ^{67}Ga decay

The decay of ^{67}Ga was followed by tracking the different γ-ray peaks in each target to estimate the half-life and activity. Figure 9(a) shows the decay curves and the half-life value obtained from each γ line. One can notice that they resemble

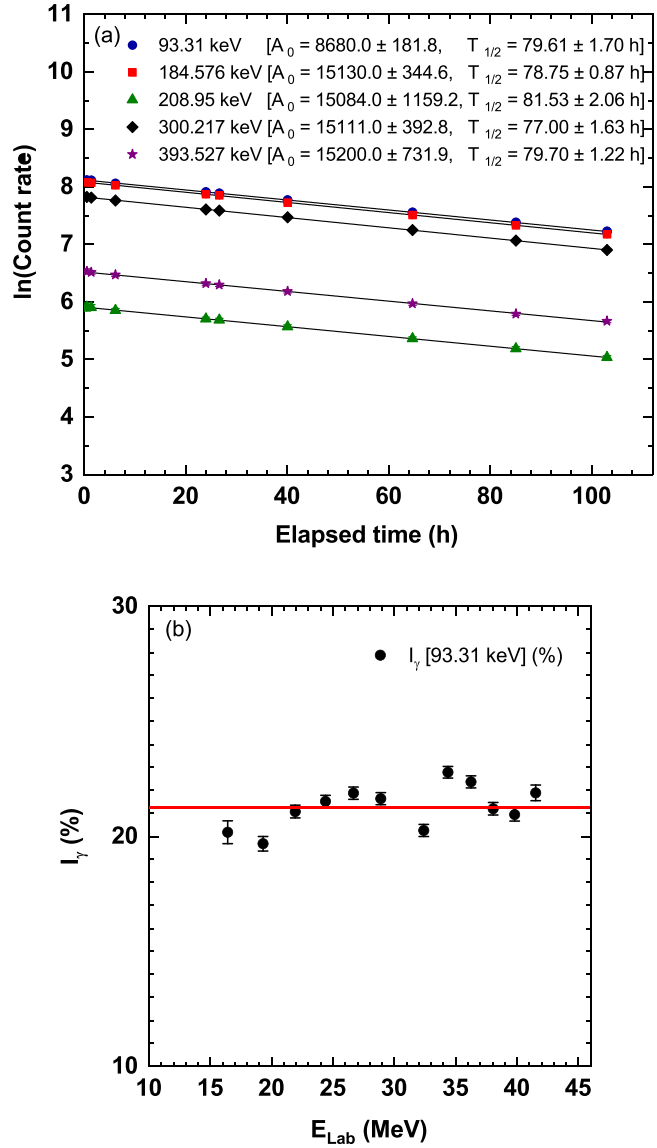

FIG. 9. Upper panel: Measured decay curves and half-life estimates of ^{67}Ga using its different γ lines from one of the target foils. $T_{1/2}$ has been calculated from the slope of the linear fit to the data, and error in $T_{1/2}$ is due to systematic uncertainty in the fitting. The equations of the linear fit to different decay curves corresponding to γ's are (i) 93.31 keV: $y = -0.0087x + 8.12$; (ii) 184.576 keV: $y = -0.0088x + 8.08$; (iii) 208.95 keV: $y = -0.0085x + 5.91$; (iv) 300.217 keV: $y = -0.009x + 7.83$; (v) 393.527 keV: $y = -0.0087x + 6.53$. The activity (A_0) is calculated using Eq. (4). Lower panel: Calculated γ-ray intensity of the 93.31 keV peak of ^{67}Ga at different energy points. The straight line represents a mean value $\langle I_\gamma \rangle = 21.3\%$.

the reported values in the available nuclear decay databases. Although similar values for half-life were obtained from different γ rays, estimated activity at the EOB corresponding to the 93.31 keV line was observed to be almost half of the value deduced using other lines [see A_0 values corresponding to different γ's in Fig. 9(a)]. A close look at the activation formula leads to an assumption that the observed inconsis-

TABLE III. Comparison of experimental half-life of ^{67}Ga and its 93.31 keV γ-line intensity with other reported values.

Database	Half-life (h)	E_γ (keV)	I_γ (%)
NuDat2.8 [50]	78.28 ± 0.012	93.31 ± 0.05	38.81 ± 0.03
LUND [61]	78.27 ± 0.014	93.311 ± 0.05	39.2 ± 1.0
NDS [62]	78.28 ± 0.012	93.31 ± 0.05	38.81 ± 0.03
JAEA [63]	78.28 ± 0.012	93.31 ± 0.05	38.81 ± 0.03
KAERI [64]	78.28 ± 0.012	93.31 ± 0.05	38.81 ± 0.03
Present work	78.60 ± 1.5	93.31	21.29 ± 0.32

tency in the measured activity is possibly due to an error in the reported intensity of the 93.31 keV γ line. Its intensity varies from 38.81% to 39.2% in different databases [50,61–64]. Using the activation formula and a simple mathematical analysis [66], the experimental intensity for 93.31 keV γ line can be estimated from the following relation:

$$A_{\mathrm{EOB}} = \frac{\lambda C_{\gamma_1}}{\varepsilon_{\gamma_1} I_{\gamma_1} e^{-\lambda T_w}(1-e^{-\lambda T_c})} = \frac{\lambda C_{\gamma_i}}{\varepsilon_{\gamma_i} I_{\gamma_i} e^{-\lambda T_w}(1-e^{-\lambda T_c})}, \tag{4}$$

where γ_1 and γ_i denote the quantities belonging to 93.31 keV and the rest of γ lines, respectively. C_γ represents the net area counts, λ is the decay constant, T_w and T_c are waiting and counting times, respectively, and ε_γ and I_γ are the efficiency and intensity, respectively, corresponding to a particular γ ray. For different γ's, the only varying quantities are the net area counts under the peak, efficiency, and intensities, such that the above equation can be reduced to

$$\frac{I_{\gamma_1}}{I_{\gamma_i}} = \frac{C_{\gamma_1}\varepsilon_{\gamma_i}}{C_{\gamma_i}\varepsilon_{\gamma_1}}. \tag{5}$$

From the above relation, intensity for the 93.31 keV line was estimated compared to other lines. Twelve targets were used in the measurement; 16 intensity values were obtained for the 93.31 keV line from each target. Hence, a total of 192 estimated values were used to determine an average experimental intensity of the 93.31 keV line. Figure 9(b) reports the estimated average experimental value of intensity at different energies corresponding to 12 targets, where the red line corresponds to the overall average of the intensity data, which happens to be 21.29 ± 0.32%. Table III presents the experimental intensity obtained from the present analysis and the reported intensities found in the nuclear databases. It can be noted that the measured half-life from the decay curve analysis is in consonance with those found in the databases. Although this problem was found unknowingly in the present reaction analysis, a dedicated experiment can be planned to determine a more precise and accurate value of the intensity of 93.31 keV γ ray from ^{67}Ga decay.

E. Production of ^{67}Ga

The ^{67}Ga (3.2617 d) radionuclide that exhibits promising application in nuclear imaging and medicine [67–70] has been produced in the ^{7}Li reaction on Cu (via the p-emitting channel). It motivates one to assess a suitable energy window for its production. Figure 10 reports the production cross sections

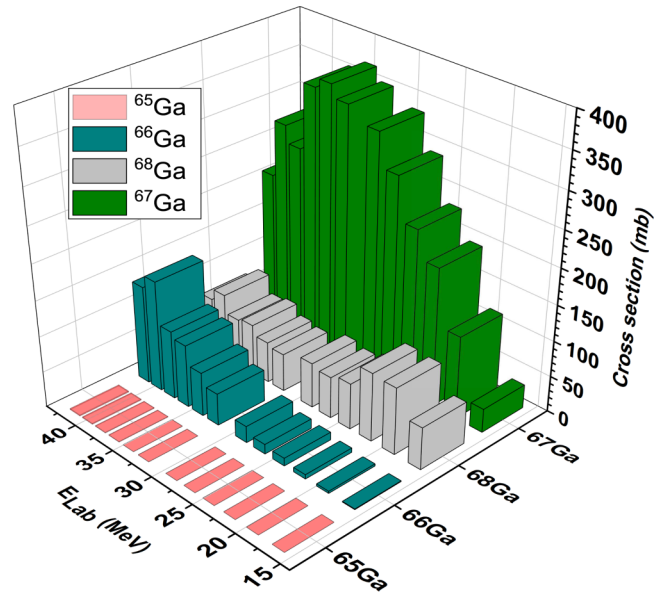

FIG. 10. The production cross sections of ^{67}Ga along with different coproduced Gallium isotopes measured in the ^{7}Li + ^{nat}Cu reaction.

of all the Ga residues measured from the p-emitting channels of the ^{7}Li + ^{nat}Cu reaction. The production of ^{67}Ga (green rectangular bars in Fig. 10) dominates over other coproduced Ga isotopes, which may be considered as isotopic impurity. It can be noted here that the cross section for ^{67}Ga peaks at 34.4 MeV (368.9 ± 32.2 mb) but also encounters sufficient production of ^{68}Ga (67.71 min) and ^{66}Ga (9.49 h) residues along with a tiny amount of ^{65}Ga (15.2 min). It is usually wise to choose an energy window to produce a desired radionuclide where less co-produced isotopes could be found. Quite fortunately, all the coproduced Ga isotopes (^{65,66,68}Ga) are short-lived compared to ^{67}Ga in the present case, and they will decay out significantly in a day, resulting in relatively pure (minimal impurity from coproduced residues) ^{67}Ga. Thus, a large energy range ≈ 20–42 MeV should be selected for the maximum production of ^{67}Ga. The use of a physical mass separator would also help to reduce isotopic impurity in the desired product, as in the case of ^{97}Ru reported recently by Kumar *et al.* [71]. However, in the present case, online mass separation would not be required in order to avoid a large amount of loss involved in the process. The coproduced radionuclides from other emission channels (Ge and Zn isotopes and bulk Cu) could be separated chemically to obtain pure ^{67}Ga tracers that would be suitable for tracer studies on the laboratory scale.

F. Coupled channel calculations

It would be interesting to note the behavior of the fusion cross section for the ^{7}Li + ^{nat}Cu reaction in comparison to the coupled channels calculations using the modified version of CCFULL code [72] to discuss the fusion scenario. CCFULL code incorporates inelastic couplings of the low-lying states of projectile and target suitably, and it also has provision for pair-transfer coupling between the ground state of interacting

TABLE IV. Potential parameters used for the ^{7}Li + ^{nat}Cu reaction along with the barrier height V_b, barrier radius R_b, and barrier curvature $\hbar\omega$.

System	Potential	V_0 (MeV)	r_0 (fm)	a (fm)	V_b (MeV)	R_b (fm)	$\hbar\omega$ (MeV)
^{7}Li + ^{63}Cu	Wood-Saxon (CC)	42.52	1.10	0.63	13.19	8.80	3.70
^{7}Li + ^{65}Cu	Wood-Saxon (CC)	42.29	1.10	0.63	13.13	8.85	3.67

nuclei, which has been dropped for the present calculation. Projectile couplings to the ^{7}Li ground state, $J^{\pi} = 3/2^{-}$ with deformation parameter $\beta = 1.189$, and the first excited state $1/2^{-}$ with $E_x^* = 0.48$ MeV, $\beta = 1.24$ [73] were included. The potential of the Wood-Saxon form under Akyuz-Winther (AW) parametrization was used in the CC calculations. The weighted averages of AW parameters are $V_0 = 42.5$ MeV, $r_0 = 1.20$ fm, and $a = 0.61$ fm. These parameters were slightly modified to fit the fusion barrier; the modified potential parameters used for coupled channel (CC) calculations, along with the uncoupled barrier heights V_b and radii R_b and curvature $\hbar\omega$, derived for the current systems, are described in Table IV. Figure 11 presents a comparison between the total fusion cross section calculated from CCFULL with and without couplings and the measured fusion cross section, which has been estimated as $\sigma_{\text{Total fusion}} = \sum\sigma_{\text{ER}} + \sum\sigma_{\text{missing ER}}$, where $\sum\sigma_{\text{ER}}$ is the sum of measured ER cross sections and $\sum\sigma_{\text{missing ER}}$ is the sum of cross sections of stable residues or the residues having very long half-lives expected to be produced via identified particle emission channels. Since the present measurement technique employed could not identify the stable or long-lived residues, the missing ER cross sections have been taken from EMPIRE with EGSM level density as it reproduced cross sections of the majority of identified residues within the energy range considered. The sums of cross sections of identified ERs and missing ERs have been tabulated in Table V. It can be seen from Fig. 11 that, far above the Coulomb barrier energies, the theoretical estimations are higher than the measured experimental ER cross sections (solid red circles). Further, it can be noted that one-dimensional barrier penetration model (1DBPM) calculations estimate cross sections slightly closer to the experimental data at lower energies. However, after incorporating the stable ER cross sections, the total cross sections (blue open circles) lie close to the 1DBPM calculations in the lower energy region, whereas $\sigma_{\text{Total Fusion}}$ lie a bit lower compared to 1DBPM on the higher energy side. On taking channel coupling in the projectile ground state ($3/2^{-}$ of ^{7}Li), it can be observed that the CC calculations quite satisfactorily reproduce the estimated fusion cross sections and lie lower than the 1DBPM calculations at energies above the Coulomb barrier. However, an enhancement compared to 1DBPM is observed below the barrier. This change in fusion cross section on taking channel couplings could be due to the fact that the ground state of ^{7}Li is quite deformed ($\beta_2 = 1.189$), leading to a reorientation effect; such an observation was observed in Ref. [18] as well. However, when the coupling of inelastic excitation to $1/2^{-}$ (first excited state) from the ground state ($3/2^{-}$) is taken, the CCFULL estimated cross sections lie lower than the experimentally estimated values at above barrier energies. At the same time, CCFULL results are satisfactory around the barrier due to the quadrupole couplings between the ground state and first excited state [$B(E2)\uparrow = 8.3\ e^2\text{fm}^4$]. The effect of inclusion of couplings to target inelastic states has been found negligible, as can be seen from Fig. 11 (green dotted curve).

G. Comparison with nearby systems

An effort has been made to compare the estimated fusion cross section for the ^{7}Li + ^{nat}Cu reaction with nearby systems employing ^{6,7}Li weakly bound projectiles. The fusion cross sections for reactions ^{6,7}Li + ^{64}Zn [17,20,33], ^{6,7}Li + ^{59}Co [18], and for the present system have been plotted as normalized cross sections ($\sigma_{fus}/\pi R^2$) as a function of $E_{\text{C.M.}}/V_b$ in Fig. 12, where $R = r_0(A_P^{1/3} + A_T^{1/3})$, A_P and A_T are the projectile and target masses respectively; here a value of $r_0 = 1.2$ fm has been used and V_b is the Coulomb barrier for a particular system. It can be well noted that the fusion cross sections of all the systems are on par with each other and establish that the presently estimated fusion cross sections lie in the

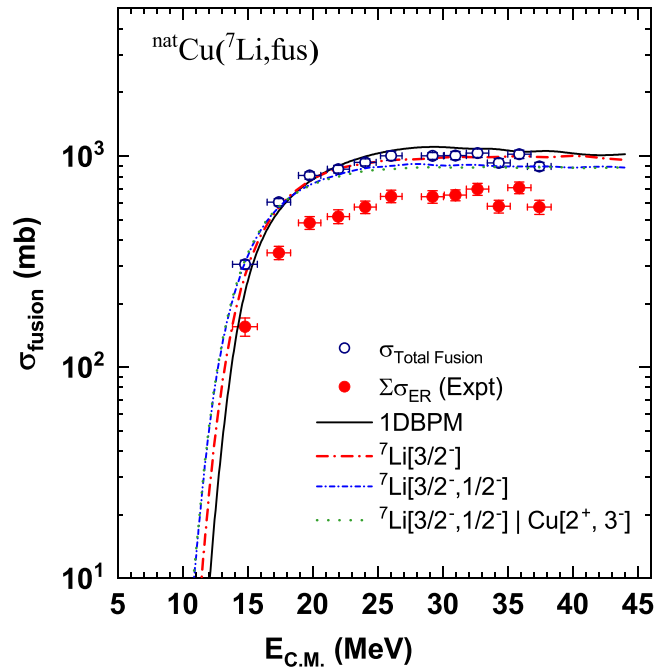

FIG. 11. Comparison of measured ER cross sections (red solid circles) and estimated fusion cross sections (blue open circles) for the ^{7}Li + ^{nat}Cu system and theoretical calculations from CCFULL with uncoupled/1DBPM (black solid curve), coupling in the projectile for the ground state $3/2^{-}$ (red dash-dot-dot curve), and inelastic coupling of the first excited state $1/2^{-}$ to the ground state (blue dash-dot curve).

TABLE V. Cross sections (mb) for identified ERs and unidentified (missing cross sections) ERs at various incident energies.

E_{Lab} (MeV)	$\sum\sigma_{ER}$ [Expt.] (mb)	$\sum\sigma_{missing\ ER}$ [EMPIRE] (mb)	σ_{Total} (mb)
16.4 ± 1.1	155.5 ± 15.3	151.0	306.5 ± 14.68
19.3 ± 1.0	347.7 ± 25.3	257.0	604.7 ± 23.9
21.9 ± 1.0	482.4 ± 33.5	326.0	808.4 ± 32.5
24.4 ± 0.9	516.2 ± 39.0	350.0	866.3 ± 35.2
26.7 ± 0.9	572.6 ± 38.5	360.0	932.6 ± 36.0
28.9 ± 0.9	643.9 ± 44.0	359.0	1002.9 ± 51.1
32.4 ± 0.9	640.8 ± 43.3	360.0	1000.8 ± 37.2
34.4 ± 0.9	652.4 ± 38.4	352.0	1004.4 ± 44.5
36.2 ± 1.0	696.3 ± 46.3	335.0	1031.3 ± 46.3
38.1 ± 1.0	577.5 ± 40.2	350.0	927.5 ± 44.3
39.8 ± 1.0	707.5 ± 44.4	313.0	1020.5 ± 47.0
41.5 ± 1.0	572.8 ± 43.8	320.0	892.8 ± 38.8

same range as those presented by the others. The fusion cross sections reported by Di Pietro *et al.* [33] lie slightly higher compared to the other mentioned data since they employed a much better technique of heavy residue (HR) identification using activation and offline atomic x-ray detection of decaying residues. They also used statistical model calculations to add the stable residue cross sections with the experimental data to get the total fusion excitation function. The vital reaction mechanism proposed by [17,18,20,33] for ^{6,7}Li reactions on medium mass targets was complete fusion with an addition of ICF/DCT channels and breakup followed by one-nucleon transfer [21]. Since these works involve comparing fusion data with coupled channels calculations or purely statistical model calculations, the PEQ mechanism is not accounted for, which could also be a contributing reaction process, as suggested by our present work.

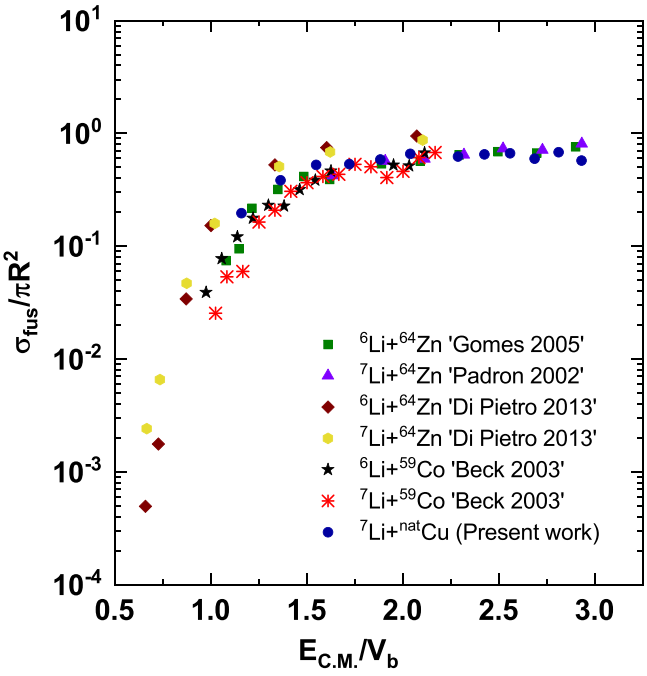

FIG. 12. Comparison of estimated fusion cross section of present reaction ^{7}Li + ^{nat}Cu (blue filled circle) with other nearby systems. The ^{6,7}Li + ^{64}Zn data were taken from Gomes *et al.* [20], Padron *et al.* [17] (green square and purple triangle), and Di Pietro *et al.* [33] (wine diamond and yellow filled circle) and those for ^{6,7}Li + ^{59}Co were taken from Beck *et al.* [18] (black star and red asterisk).

V. CONCLUSION

This article reports the measured cross sections of a total of ten residues, ^{69,67,66}Ge, ^{68,67,66,65}Ga, and ^{69m,65,63}Zn, for the first time, from the ^{7}Li + ^{nat}Cu reaction within 16–42 MeV energy. The cross sections have been compared with the theoretical model calculations based on the EQ and PEQ mechanisms under the framework of EMPIRE-3.2.2 nuclear reaction code. Overall, a mixture of both EQ and PEQ models leads to a better justification of the measured data. An estimate of the experimental intensity of 93.31 keV γ line has been reported following the trend of measured EOB activity from other γ lines of ^{67}Ga decay. No significant evidence of ICF in the proton/α channels was observed in this reaction which could be unambiguously differentiated from CF, possibly due to the target's light charge and a higher breakup threshold of ^{7}Li too. The production possibility of ^{67}Ga has been put forth using the ^{7}Li + ^{nat}Cu reaction. A coupled channels analysis was performed to understand the fusion mechanism of the ^{7}Li + ^{nat}Cu reaction; the experimental fusion cross sections were adequately explained by incorporating inelastic couplings in the projectile. The present cross section data are in line with those reported from other nearby systems, emphasizing the validity of the fusion data and suggesting that complete fusion is the underlying reaction mechanism for ^{7}Li reactions on medium mass targets. A discrepancy between model calculations and experimental data for ^{67}Ga was observed, which certainly demands more experimental data for ^{7}Li induced reactions on targets in the same mass region as Cu that would populate ^{67}Ga from different emission channels, to make a thorough understanding of such processes.

ACKNOWLEDGMENTS

The authors are thankful to the BARC-TIFR Pelletron staff for their cooperation and help during the experiment. We also appreciate our colleagues from the TASISPEC Lab of IIT Roorkee for their ardent teamwork in the learning phase. Research Grant No. CRG/2018/002354 from SERB(IN) and support via research fellowships from DST-INSPIRE (IF180078) funded by Department of Science and Technology, Ministry of Science and Technology, Government of India, are gratefully acknowledged. We acknowledge the support of the Department of Atomic Energy, Government of India, under Project No. 12P-R&D-TFR-5.02-0300.

[1] M. Trotta, A. M. Stefanini, S. Beghini, B. R. Behera, A. Yu. Chizhov, L. Corradi, S. Courtin, E. Fioretto, A. Gadea, P. R. S. Gomes, F. Haas, I. M. Itkis, M. G. Itkis, G. N. Kniajeva, N. A. Kondratiev, E. M. Kozulin, A. Latina, G. Montagnoli, I. V. Pokrovsky, N. Rowley, R. N. Sagaidak, F. Scarlassara, A. Szanto de Toledo, S. Szilner, V. M. Voskressensky, and Y. W. Wu, Eur. Phys. J. A **25**, 615 (2005).

[2] V. F. Weisskopf, Phys. Rev. **52**, 295 (1937).

[3] M. Blann, Annu. Rev. Nucl. Sci. **25**, 123 (1975).

[4] E. Holub, D. Hilscher, G. Ingold, U. Jahnke, H. Orf, and H. Rossner, Phys. Rev. C **28**, 252 (1983).

[5] M. Cavinato, E. Fabrici, E. Gadioli, E. Gadioli Erba, P. Vergani, M. Crippa, G. Colombo, I. Redaelli, and M. Ripamonti, Phys. Rev. C **52**, 2577 (1995).

[6] M. K. Sharma, P. P. Singh, D. P. Singh, A. Yadav, V. R. Sharma, I. Bala, R. Kumar, Unnati, B. P. Singh, and R. Prasad, Phys. Rev. C **91**, 014603 (2015).

[7] D. Kumar, M. Maiti, and S. Lahiri, Phys. Rev. C **94**, 044603 (2016).

[8] R. Prajapat, M. Maiti, D. Kumar, and A. Chauhan, Phys. Scr. **95**, 055306 (2020).

[9] H. C. Britt and A. R. Quinton, Phys. Rev. **124**, 877 (1961).

[10] J. Galin, B. Gatty, D. Guerreau, C. Rousset, U. C. Schlotthauer-Voos, and X. Tarrago, Phys. Rev. C **9**, 1126 (1974).

[11] T. Inamura, M. Ishihara, T. Fukuda, T. Shimoda, and H. Hiruta, Phys. Lett. B **68**, 51 (1977).

[12] D. J. Hinde, M. Dasgupta, B. R. Fulton, C. R. Morton, R. J. Wooliscroft, A. C. Berriman, and K. Hagino, Phys. Rev. Lett. **89**, 272701 (2002).

[13] H. Esbensen, Phys. Rev. C **81**, 034606 (2010).

[14] P. R. S. Gomes, R. Linares, J. Lubian, C. C. Lopes, E. N. Cardozo, B. H. F. Pereira, and I. Padron, Phys. Rev. C **84**, 014615 (2011).

[15] B. B. Back, H. Esbensen, C. L. Jiang, and K. E. Rehm, Rev. Mod. Phys. **86**, 317 (2014).

[16] V. Jha, V. V. Parkar, and S. Kailas, Phys. Rep. **845**, 1 (2020).

[17] I. Padron, P. R. S. Gomes, R. M. Anjos, J. Lubian, C. Muri, J. J. S. Alves, G. V. Marti, M. Ramírez, A. J. Pacheco, O. A. Capurro, J. O. Fernández Niello, J. E. Testoni, D. Abriola, and M. R. Spinella, Phys. Rev. C **66**, 044608 (2002).

[18] C. Beck, F. A. Souza, N. Rowley, S. J. Sanders, N. Aissaoui, E. E. Alonso, P. Bednarczyk, N. Carlin, S. Courtin, A. Diaz-Torres, A. Dummer, F. Haas, A. Hachem, K. Hagino, F. Hoellinger, R. V. F. Janssens, N. Kintz, R. Liguori Neto, E. Martin, M. M. Moura, M. G. Munhoz, P. Papka, M. Rousseau, A. Sanchez i Zafra, O. Stezowski, A. A. Suaide, E. M. Szanto, A. Szanto de Toledo, S. Szilner, and J. Takahashi, Phys. Rev. C **67**, 054602 (2003).

[19] M. Dasgupta, P. R. S. Gomes, D. J. Hinde, S. B. Moraes, R. M. Anjos, A. C. Berriman, R. D. Butt, N. Carlin, J. Lubian, C. R. Morton, J. O. Newton, and A. Szanto de Toledo, Phys. Rev. C **70**, 024606 (2004).

[20] P. R. S. Gomes, M. D. Rodríguez, G. V. Martí, I. Padron, L. C. Chamon, J. O. Fernández Niello, O. A. Capurro, A. J. Pacheco, J. E. Testoni, A. Arazi, M. Ramírez, R. M. Anjos, J. Lubian, R. Veiga, R. Liguori Neto, E. Crema, N. Added, C. Tenreiro, and M. S. Hussein, Phys. Rev. C **71**, 034608 (2005).

[21] A. Shrivastava, A. Navin, N. Keeley, K. Mahata, K. Ramachandran, V. Nanal, V. V. Parkar, A. Chatterjee, and S. Kailas, Phys. Lett. B **633**, 463 (2006).

[22] C. S. Palshetkar, S. Thakur, V. Nanal, A. Shrivastava, N. Dokania, V. Singh, V. V. Parkar, P. C. Rout, R. Palit, R. G. Pillay, S. Bhattacharyya, A. Chatterjee, S. Santra, K. Ramachandran, and N. L. Singh, Phys. Rev. C **89**, 024607 (2014).

[23] V. V. Parkar, S. K. Sharma, R. Palit, S. Upadhyaya, A. Shrivastava, S. K. Pandit, K. Mahata, V. Jha, S. Santra, K. Ramachandran, T. N. Nag, P. K. Rath, B. Kanagalekar, and T. Trivedi, Phys. Rev. C **97**, 014607 (2018).

[24] S. Kalkal, E. C. Simpson, D. H. Luong, K. J. Cook, M. Dasgupta, D. J. Hinde, I. P. Carter, D. Y. Jeung, G. Mohanto, C. S. Palshetkar, E. Prasad, D. C. Rafferty, C. Simenel, K. Vo-Phuoc, E. Williams, L. R. Gasques, P. R. S. Gomes, and R. Linares, Phys. Rev. C **93**, 044605 (2016).

[25] G. L. Zhang, G. X. Zhang, S. P. Hu, Y. J. Yao, J. B. Xiang, H. Q. Zhang, J. Lubian, J. L. Ferreira, B. Paes, E. N. Cardozo, H. B. Sun, J. J. Valiente-Dobon, D. Testov, A. Goasduff, P. R. John, M. Siciliano, F. Galtarossa, R. Francesco, D. Mengoni, D. Bazzacco, E. T. Li, X. Hao, and W. W. Qu, Phys. Rev. C **97**, 014611 (2018).

[26] D. H. Luong, M. Dasgupta, D. J. Hinde, R. du Rietz, R. Rafiei, C. J. Lin, M. Evers, and A. Diaz-Torres, Phys. Lett. B **695**, 105 (2011).

[27] L. F. Canto, P. R. S. Gomes, R. Donangelo, J. Lubian, and M. S. Hussein, Phys. Rep. **596**, 1 (2015).

[28] R. Raabe, C. Angulo, J. L. Charvet, C. Jouanne, L. Nalpas, P. Figuera, D. Pierroutsakou, M. Romoli, and J. L. Sida, Phys. Rev. C **74**, 044606 (2006).

[29] S. P. Hu, G. L. Zhang, J. C. Yang, H. Q. Zhang, P. R. S. Gomes, J. Lubian, X. G. Wu, J. Zhong, C. Y. He, Y. Zheng, C. B. Li, G. S. Li, W. W. Qu, F. Wang, L. Zheng, L. Yu, Q. M. Chen, P. W. Luo, H. W. Li, Y. H. Wu, W. K. Zhou, B. J. Zhu, and H. B. Sun, Phys. Rev. C **91**, 044619 (2015).

[30] D. Kumar, M. Maiti, and S. Lahiri, Phys. Rev. C **96**, 014617 (2017).

[31] A. Chauhan and M. Maiti, Phys. Rev. C **99**, 034608 (2019).

[32] R. Prajapat and M. Maiti, Phys. Rev. C **103**, 034620 (2021).

[33] A. Di Pietro, P. Figuera, E. Strano, M. Fisichella, O. Goryunov, M. Lattuada, C. Maiolino, C. Marchetta, M. Milin, A. Musumarra, V. Ostashko, M. G. Pellegriti, V. Privitera, G. Randisi, L. Romano, D. Santonocito, V. Scuderi, D. Torresi, and M. Zadro, Phys. Rev. C **87**, 064614 (2013).

[34] M. F. Guo, G. L. Zhang, P. R. S. Gomes, J. Lubian, and E. Ferioli, Phys. Rev. C **94**, 044605 (2016).

[35] R. Prajapat and M. Maiti, Phys. Rev. C **101**, 064620 (2020).

[36] R. Prajapat and M. Maiti, Phys. Rev. C **101**, 024608 (2020).

[37] A. Chauhan, M. Maiti, and S. Lahiri, Phys. Rev. C **99**, 064609 (2019).

[38] A. Chauhan, R. Prajapat, G. Sarkar, M. Maiti, R. Kumar, Malvika, Gonika, J. Gehlot, S. Nath, A. Parihari, and N. Madhavan, Phys. Rev. C **102**, 064606 (2020).

[39] M. Sagwal, M. Maiti, T. N. Nag, and S. Sodaye, Eur. Phys. J. Plus **136**, 1057 (2021).

[40] M. Maiti and S. Lahiri, Phys. Rev. C **84**, 067601 (2011).

[41] M. Maiti, Phys. Rev. C **84**, 044615 (2011).

[42] R. Prajapat and M. Maiti, J. Radioanal. Nucl. Chem. **325**, 757 (2020).

[43] M. Maiti and S. Lahiri, Radiochim. Acta **103**, 7 (2015).

[44] M. Maiti, S. Lahiri, and B. S. Tomar, Radiochim. Acta **99**, 527 (2011).

[45] M. Maiti, Radiochim. Acta **101**, 437 (2013).
[46] M. Maiti, S. Lahiri, and B. S. Tomar, J. Radioanal. Nucl. Chem. **288**, 115 (2011).
[47] J. F. Ziegler, M. D. Ziegler, and J. P. Biersack, Nucl. Instrum. Methods Phys. Res. B **268**, 1818 (2010).
[48] M. Maiti and S. Lahiri, Phys. Rev. C **81**, 024603 (2010).
[49] R. Prajapat, M. Maiti, and D. Kumar, Phys. Rev. C **103**, 014608 (2021).
[50] National Nuclear Data Center, Brookhaven National Laboratory, http://www.nndc.bnl.gov/nudat2/ (Accessed on 19 May 2021).
[51] B. Wilken and T. A. Fritz, Nucl. Instrum. Methods **138**, 331 (1976).
[52] M. Herman, R. Capote, B. V. Carlson, P. Oblozinsky, M. Sin, A. Trkov, H. Wienke, and V. Zerkin, Nucl. Data Sheets **108**, 2655 (2007).
[53] C. H. Dasso and S. Landowne, Comput. Phys. Commun. **46**, 187 (1987).
[54] A. J. Koning and J. P. Delaroche, Nucl. Phys. A **713**, 231 (2003).
[55] H. An and C. Cai, Phys. Rev. C **73**, 054605 (2006).
[56] F. D. Becchetti, Jr. and G. W. Greenless, Phys. Rev. **182**, 1190 (1969).
[57] V. Avrigeanu, P. E. Hodgson, and M. Avrigeanu, Phys. Rev. C **49**, 2136 (1994).
[58] A. V. Ignatyuk, G. N. Smirenkin, and A. S. Tishin, Sov. J. Nucl. Phys. **21**, 255 (1975) [Yad. Fiz. **21**, 485 (1975)].
[59] P. G. Young, E. D. Arthur, M. Bozoian, T. R. England, G. M. Hale, R. J. LaBauve, R. C. Little, R. E. MacFarlane, D. G. Madland, R. T. Perry, and W. B. Wilson, Trans. Am. Nucl. Soc. **60**, 271 (1989).
[60] A. S. Iljinov, M. V. Mebel, N. Bianchi, E. De Sanctis, C. Guaraldo, V. Lucherini, V. Muccifora, E. Polli, A. R. Reolon, and P. Rossi, Nucl. Phys. A **543**, 517 (1992).
[61] S. Y. F. Chu, L. P. Ekstrom, and R. B. Firestone, WWW Table of Radioactive Isotopes, The Lund/LBNL Nuclear Data Search, 1999, http://nucleardata.nuclear.lu.se/toi/ (Accessed on 19 May 2021).
[62] Live Chart of Nuclides: Nuclear Structure and Decay Data, NDS, IAEA, 2019, https://www-nds.iaea.org/relnsd/vcharthtml/VChartHTML.html (Accessed on 19 May 2021).
[63] WWW Chart of the Nuclides, Japanese Nuclear Data Library, 2014, https://wwwndc.jaea.go.jp/CN14/index.html (Accessed on 19 May 2021).
[64] Table of γ-rays, Nuclear Data Center, Korean Atomic Energy Research Institute (KAERI), 2015, http://atom.kaeri.re.kr/ (Accessed on 19 May 2021).
[65] R. Kumar, M. Maiti, G. Sarkar, M. Sagwal, P. Kaur, R. Prajapat, T. N. Nag, and S. Sodaye, Eur. Phys. J. A **57**, 209 (2021).
[66] B. M. Ali, G. Y. Mohamed, F. Ditrói, S. Takács, and M. Al-Abyad, Phys. Rev. C **102**, 064608 (2020).
[67] S. M. Qaim, Nucl. Med. Biol. **44**, 31 (2017).
[68] S. Lahiri and S. Sarkar, Appl. Radiat. Isot. **65**, 309 (2007).
[69] E. Koumarianou, T. A. Slastnikova, M. Pruszynski, A. A. Rosenkranz, G. Vaidyanathan, A. S. Sobolev, and M. R. Zalutsky, Nucl. Med. Biol. **41**, 441 (2014).
[70] D. M. Lesk, T. E. Wood, S. E. Carroll, and L. Reese, Radiology **128**, 707 (1978).
[71] D. Kumar, M. Maiti, R. Prajapat, A. Chauhan, R. Biswas, J. Gehlot, S. Nath, R. Kumar, N. Madhavan, G. N. Jyothi, R. N. Sahoo, M. M. Shaikh, and V. Srivastava, Phys. Rev. C **104**, 014602 (2021).
[72] K. Hagino, N. Rowley, and A. T. Kruppa, Comput. Phys. Commun. **123**, 143 (1999).
[73] P. K. Rath, S. Santra, N. L. Singh, B. K. Nayak, K. Mahata, R. Palit, K. Ramachandran, S. K. Pandit, A. Parihari, A. Pal, S. Appannababu, S. K. Sharma, D. Patel, and S. Kailas, Phys. Rev. C **88**, 044617 (2013).